EJN fens EUROPEAN JOURNAL OF NEUROSCIENCE

European Journal of Neuroscience, Vol. 33, pp. 1433–1444, 2011 doi:10.1111/j.1460-9568.2010.07597.x

MOLECULAR AND DEVELOPMENTAL NEUROSCIENCE

The increased density of p38 mitogen-activated protein kinase-immunoreactive microglia in the sensorimotor cortex of aged TgCRND8 mice is associated predominantly with smaller dense-core amyloid plaques

J. Chlan-Fourney,[1] T. Zhao,[2,3] W. Walz[3] and D. D. Mousseau[2,3]
[1]Department of Anatomy and Cell Biology, University of Saskatchewan, Saskatoon, SK, Canada
[2]Cell Signalling Laboratory, B45 HSB, University of Saskatchewan, 107 Wiggins Road, Saskatoon, SK S7N 5E5, Canada
[3]Department of Psychiatry, University of Saskatchewan, Saskatoon, SK, Canada

Keywords: Alzheimer's disease, dementia, Macrophage-1(CD11b/CD18), microglia, p38 mitogen-activated protein kinase, stereology

Abstract

The role for phosphorylated p38 mitogen-activated protein kinase [p-p38(MAPK)] in β-amyloid plaque deposition [a hallmark of Alzheimer's disease (AD) pathology] remains ambiguous. We combined immunohistochemistry and stereological sampling to quantify the distribution of plaques and p-p38(MAPK)-immunoreactive (IR) cells in the sensorimotor cortex of 3-, 6- and 10-month-old TgCRND8 mice. The aggressive nature of the AD-related human amyloid-β protein precursor expressed in these mice was confirmed by the appearance of both dense-core (thioflavin-S-positive) and diffuse plaques, even in the youngest mice. p-p38(MAPK)-IR cells of the sensorimotor cortex were predominantly co-immunoreactive for the Macrophage-1 (CD11b/CD18) microglial marker. These p-p38(MAPK)-IR microglia were associated with both dense-core and diffuse plaques, but the expected age-dependent increase in the density of plaque-associated p-p38(MAPK)-IR microglia was restricted to dense-core plaques. Furthermore, the density of dense-core plaque-associated p-p38(MAPK)-IR microglia was inversely correlated with the size of the core within the given plaque, which supports a role for these microglia in restricting core growth. p-p38(MAPK)-IR microglia were also observed throughout wildtype and TgCRND8 mouse cortical parenchyma, but the density of these non-plaque-associated microglia remained constant, regardless of age or genotype. We conclude that the constitutive presence of p-p38(MAPK)-IR microglia in aging mouse brain is indicative of a longitudinal role for this kinase in normal brain physiology. We suggest that this fact, as well as the fact that a pool of p-p38(MAPK)-IR microglia appears to restrict β-amyloid plaque core development, needs to be duly considered when ascribing functions for p38(MAPK) signalling in the AD brain.

Introduction

Neuropathological hallmarks of Alzheimer's disease (AD) include senile plaques and neurofibrillary tangles in the hippocampus (Probst *et al.*, 1982) and cortex (Pearson *et al.*, 1985). Senile plaques can be classified grossly as 'diffuse' plaques, which have very little of the β-sheet/fibrillar conformation of the β-amyloid (Aβ) peptide, and 'dense-core' plaques, which are identified by β-sheet-sensitive dyes including thioflavin-S. The remnants of nuclear elements, such as nucleotides and/or ATP/ADP (Neary *et al.*, 1996; D'Andrea *et al.*, 2001; Honda *et al.*, 2001), contribute to microglial chemotaxis, and undoubtedly account for the preferential association of activated microglia with dense-core plaques (Stalder *et al.*, 1999). Microglia potentially play a positive role, by way of Aβ clearance and the restriction of plaque size (Simard *et al.*, 2006; El Khoury *et al.*, 2007; Grathwohl *et al.*, 2009), and a negative role, as purveyors of inflammation (Hanisch & Kettenmann, 2007), during the progression of AD.

The enzyme p38 mitogen-activated protein kinase [p38(MAPK)], particularly its phosphorylated form [p-p38(MAPK)], has been detected in vulnerable regions of the AD brain, including the hippocampus and cortex (Hensley *et al.*, 1999; Koistinaho *et al.*, 2002). However, although p38(MAPK) has been associated with apoptosis *in vitro* (Wada & Penninger, 2004), its role in neuronal apoptosis *in vivo* remains ambiguous. Indeed, p38(MAPK) is constitutively activated in the cortex, hippocampus and cerebellum (Lee *et al.*, 2000), and p38(MAPK) signalling has been shown to enhance survival (Park *et al.*, 2002), cell growth (Juretic *et al.*, 2001) and differentiation (Morooka & Nishida, 1998; Yosimichi *et al.*, 2001). p38(MAPK) activation has been observed in early stages of AD, when markers of apoptosis are uncharacteristically absent (Zhu *et al.*, 2003). Furthermore, stress-associated activation of p38(MAPK) actually renders AD fibroblasts resistant to a subsequent apoptotic challenge

Correspondence: D. D. Mousseau, [2]Cell Signalling Laboratory, as above.
E-mail: darrell.mousseau@usask.ca

Received 6 September 2010, revised 7 December 2010, accepted 20 December 2010

(Naderi *et al.*, 2006), induces antioxidant proteins (Premkumar *et al.*, 1995) and inhibits pro-oxidative enzymes (Cao *et al.*, 2009).

The ambiguity is further fuelled by reports of dense-core plaque-associated p-p38(MAPK)-positive microglia and astrocytes (Frautschy *et al.*, 1998; Bellucci *et al.*, 2007; Giovannini *et al.*, 2008) in animal models of AD-related amyloidosis. The neocortex and hippocampus of the TgCRND8 mouse model of amyloidosis contain plaque-associated cells that are immunoreactive for activated stress-associated protein kinase/c-*jun* N-terminal kinase (Bellucci *et al.*, 2007) and p-p38(MAPK) (Giovannini *et al.*, 2008), and that are believed to play detrimental roles in plaque development. The current series of experiments combined immunohistochemistry and quantitative (stereological) sampling to examine the association between p-p38(MAPK) and plaques in the TgCRND8 mouse sensorimotor cortex, a region that is particularly vulnerable during the progression of clinical AD (Frisoni *et al.*, 2009). Our analyses confirm an association between p-p38(MAPK)-immunoreactive (IR) microglia and dense-core plaques, but also reveal an age-dependent, inverse relation between the density of these microglia and plaque core size. Given the region-dependent differences in p-p38(MAPK)-IR cell phenotype and function in the AD mouse sensorimotor cortex (current study) and hippocampus (Bellucci *et al.*, 2007; Giovannini *et al.*, 2008), a thorough understanding of p38(MAPK) signalling in AD-related amyloidosis is certainly warranted.

Materials and methods

The $APP_{Swe/Ind}$ TgCRND8 mice

All procedures were performed in accordance with the Canadian Council on Animal Care guidelines and were approved by the University of Saskatchewan Animal Care Committee. TgCRND8 mice are a model of aggressive AD-related amyloidosis as they express a transgene incorporating both the Indiana mutation (V717F) and the Swedish mutations (K670N/M671L) in the human amyloid-β protein precursor (APP) gene (Chishti *et al.*, 2001). These mice were obtained from the Centre for Research in Neurodegenerative Diseases (University of Toronto, Toronto, ON, Canada).

Antibodies

Rabbit anti-p-p38(MAPK) (#9211) and mouse anti-total p38(MAPK) (#9217) were purchased from Cell Signaling Technology (Danvers, MA, USA); mouse anti-neuronal-specific antibody (NeuN) (clone A60; MAB377) was obtained from Millipore (Billerica, MA, USA); mouse anti-glial fibrillary acidic protein (GFAP) (G3893) was obtained from Sigma-Aldrich Ltd (St Louis, MO, USA); mouse anti-APP (clone 6E10; SIG 39320) was purchased from Covance (Princeton, NJ, USA); and mouse anti-Macrophage-1 (CD11b/CD18) (Mac-1)/anti-CD11b (MCA74G) and mouse anti-ectodermal dysplasia-1 (CD68) (ED-1)/anti-CD68 (MCA341R) were obtained from Serotec (Raleigh, NC, USA).

Tissue preparation and histology

The 3-, 6- and 10-month-old TgCRND8 and wildtype (WT) male and female mice (n = 4–5 animals per group) were killed with sodium pentobarbital (50 mg/kg i.p.) and prepared for immunohistochemical studies by transcardiac perfusion with cold 0.1 M phosphate-buffered saline (PBS; pH 7.4). Brains were removed, rinsed in PBS and post-fixed for 24 h in 4% paraformaldehyde. They were transferred to 30% glycerol/0.1 M phosphate buffer for 48 h and then flash-frozen and stored at −70 °C until sectioned coronally (30 μm). Every sixth section was used for the determination of Aβ plaque distribution, size and type. Plaques were classified as dense core (immunoreactive for the anti-APP 6E10 antibody as well as positive for thioflavin-S-positive staining) or diffuse (immunoreactive for the anti-APP 6E10 antibody, but negative for thioflavin-S staining). The remaining sections were processed for thionin/Nissl staining, immunohistochemistry or immunofluorescence.

Immunohistochemistry

Free-floating sections were incubated in 10 mM sodium citrate buffer at 70 °C for 30 min and for an additional 30 min at room temperature (RT, 20°C) for antigen retrieval. Sections were then immersed for 30 min in 0.2% H_2O_2 to inhibit endogenous peroxidase activity and blocked for 2 h (RT) with 5% normal serum in PBS/0.3% Triton X-100. Sections were incubated for 72 h at 4 °C and then for 2 h at RT in PBS/0.3% Triton X-100 (+1% normal serum) with anti-p-p38(MAPK) at 1 : 100. Sections were then blocked with 2.5% normal serum in PBS/0.3% Triton X-100 and incubated (1 h, RT) with goat anti-rabbit (BA1000; Vector Laboratories, Inc., Burlington, ON, Canada) secondary antibody (1 : 250). The sections were processed by the avidin–biotin–peroxidase/3,3′-diaminobenzidine (DAB) method (Vector Laboratories, Inc.). Each step was followed by three washes (20 min, RT) in PBS. Sections mounted on gelatin-coated slides were stained with either 1% thioflavin-S (Sigma-Aldrich Ltd) for 5 min for the detection of β-sheet-rich Aβ-containing plaques, or thionin (Nissl). Sections were coverslipped with ProLong® Gold Fluorescent Mounting Media (P36930; Invitrogen, Carlsbad, CA, USA).

Indirect immunofluorescence

Sections were treated for antigen retrieval and then blocked in normal serum and placed in primary and secondary antibody solutions as described above. Free-floating sections were processed for double immunofluorescence with anti-p-p38(MAPK) paired with the following individual antibodies: 6E10 (reacts to amino acid residues 1–16 of the Aβ peptide; 1 : 1000); Mac-1 (also called CD11b or OX-42; recognizes the rat equivalent of the human complement receptor type 3 that is present on the cell membrane of macrophages, as well as most resident and active microglia, and preferentially stains cellular processes and the cytoplasmic cell membrane; 1 : 100); ED-1 (also called CD68 or macrosialin; recognizes the rat equivalent of the human CD68 that is expressed primarily on the lysosomal membrane of myeloid cells such as macrophages, and therefore produces primarily cytoplasmic staining; 1 : 100); NeuN (1 : 100); and GFAP (recognizes astrocytes; 1 : 5000). Secondary antibodies (1 : 500) included Alexa Fluor® (Invitrogen) 488 goat anti-mouse, 488 goat anti-rabbit, 555 goat anti-mouse, 555 goat anti-rabbit and 594 goat anti-rabbit. All experiments included control sections incubated in the absence of primary antibody (see example in Fig. 1B).

Stereological quantitative analysis

The number of p-p38(MAPK)-IR cells in the sensorimotor cortex of WT and TgCRND8 mice was quantified with STEREO INVESTIGATOR software (MicroBrightField, Inc., Williston, VT, USA) under a 40× objective using the Optical Fractionator stereological technique. Every 12th section was selected from the total number of sections containing the sensorimotor cortex that were between Bregma 0.74 and −1.70

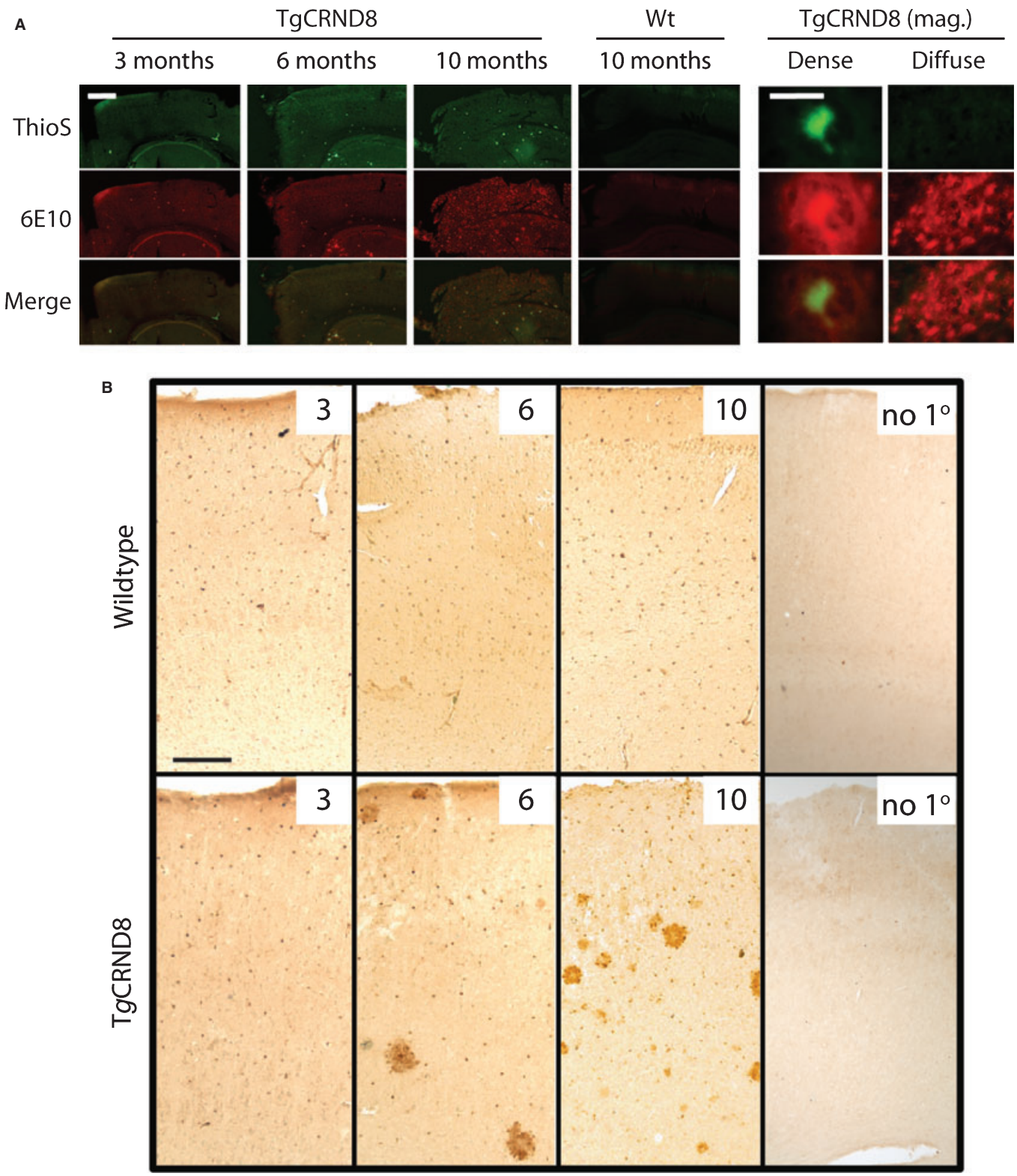

FIG. 1. The distribution of p-p38(MAPK)-IR cells in the sensorimotor cortex of TgCRND8 mice of increasing age. (A) Representative photomicrographs (scale bar, 400 μm) of progressive APP expression and Aβ deposition in coronal sections of the sensorimotor cortex of TgCRND8 mice (at 3, 6 and 10 months of age). Fibrillar Aβ is revealed by thioflavin-S staining, whereas APP/Aβ expression is revealed by 6E10 immunofluorescence. A section from a 10-month-old WT mouse is included for comparison. TgCRND8 (mag.), Magnification of a dense-core and a diffuse Aβ plaque show a clear difference in thioflavin-S staining and 6E10 patterning (scale bar, 10 μm). (B) DAB immunohistochemistry was used to examine the distribution of p-p38(MAPK) immunoreactivity in the sensorimotor cortex of WT and TgCRND8 mice. DAB immunohistochemistry revealed patches that were clearly evident in the sections from 6- and 10-month-old TgCRND8 cortex and revealed an increased number of p-p38(MAPK)-IR cells in the immediate vicinity of what are undoubtedly Aβ deposits/plaques. no 1°, no primary, i.e. 'control' DAB immunohistochemistry in the absence of primary antibody (but incubated with secondary antibody). Scale bar, 100 μm.

(Franklin & Paxinos, 1997), and processed for p-p38(MAPK) DAB immunohistochemistry. A preliminary population estimate was performed to determine the optimal counting-frame size, counting-frame spacing and total number of sections to sample for the density of p-p38(MAPK)-IR cells present in the brain parenchyma, i.e. those p-p38(MAPK)-IR cells that appeared to be evenly distributed throughout the cortex and were not associated with (i.e. not in contact with) Aβ plaques. This preliminary estimate revealed that a section periodicity of 12 (e.g. 1 in 12 sections) would result in a sampling of six sections per animal and would be sufficient to bring the coefficient of error in sampling variance to < 0.05 (Scheaffer *et al.*, 1996), provided that the X and Y dimensions of the counting-frame were 100 μm^2 in a 150 μm^2 counting grid. The section thickness (measured in the Z axis) averaged 14 μm and therefore p-p38(MAPK)-IR cells were counted through a depth of 12 μm, leaving a 2 μm guard zone.

Boundaries of the mouse sensorimotor cortex (Franklin & Paxinos, 1997) on thionin-stained sections were traced using STEREO INVESTIGATOR software across all six layers of the cortex. Upon initial inspection of p-p38(MAPK)-IR cells in the TgCRND8 mice at all three ages, it became apparent that a clustering of three or more p-p38(MAPK)-IR cells was a reliable marker of Aβ plaques in this animal model, which we confirmed by subsequently co-localizing p-p38(MAPK) immunoreactivity with both thioflavin-S and 6E10. These p-p38(MAPK)-IR cells were counted as 'plaque-associated p-p38(MAPK)-IR cells' only if they were in direct contact with a plaque. Mean cell counts (MCCs) (mean number of cells/unit volume) of the density of p-p38(MAPK)-IR cells that were not associated with Aβ plaques were also estimated across the cortex in six sections to bring the coefficient of error in sampling variance to < 0.05 (Scheaffer *et al.*, 1996). These p-p38(MAPK)-IR cells were counted if they were distributed throughout the parenchyma and if they were not in a cluster of p-p38(MAPK)-IR cells, and will be referred to hereinafter as 'parenchymal' p-p38(MAPK)-IR cells. Therefore, we were able to simultaneously sample for plaque-associated p-p38(MAPK)-IR cells and resident (parenchymal) p-p38(MAPK)-IR cells (using two different markers in the STEREO INVESTIGATOR software). Although we would have preferred to report the total number of cells estimated by the Optical Fractionator (instead of only the MCCs, or cell densities), the condition of the fixed TgCRND8 tissue, due to its fragile nature, did not allow for tracing of the entire sensorimotor cortex in all sections.

Post-hoc semi-quantitative analysis

The 6E10 antibody was used to estimate plaque diameters. As the thionin stain provided a reliable marker of what we subsequently confirmed were thioflavin-S-positive cores, we were able to approximate the size of the core in a given plaque. The total plaque and core areas were estimated by making two measurements of plaque/core diameters, with one measure being made through the midpoint of the plaque across its widest aspect, and the second measure being perpendicular to the first and also through the midpoint. Sets of sections were analysed blindly and independently by J.C.-F. and T.Z. This approach allowed us to measure the absolute core size as well as the proportional core size, i.e. defined as the ratio of the area occupied by the core vs. the total area occupied by the plaque.

Determination of the phenotype of p-p38(MAPK)-immunoreactive cells using confocal microscopy

The distribution of p-p38(MAPK) immunoreactivity around 6E10-IR aggregates was confirmed using a confocal microscope equipped with a BX71 Olympus microscope and FluoView SV500 imaging software using a 40× air objective. In order to determine the type of cells that were p-p38(MAPK)-IR, sections were also processed for double immunofluorescence for NeuN (neurons), GFAP (astrocytes), Mac-1 (monocytes/microglia) or ED-1 (monocytes/microglia) in 10-month-old TgCRND8 mice using a 60× oil immersion lens. Double immunofluorescence for p-p38(MAPK) and total p38(MAPK) was obtained using a 100× oil immersion lens. The two transmission channels (from the Ar and He lasers) were captured at the same time and filtered by eight Kalman low-speed scans. Thin optical sections were used for all images, with each step in the z-axis being 1.0 μm through a range of 5.0 μm, with the most representative image being saved. For images of 6E10 and p-p38(MAPK) double immunofluorescence, a similar series of images were obtained under a 100× oil immersion lens and a series of three photographs (step, 1.0 μm) were captured.

Statistics

Significance was set at $P < 0.05$. Two-way ANOVA was used to compare how the MCC of plaque-associated and/or parenchymal p-p38(MAPK)-IR cells varied as a function of age and genotype (i.e. Fig. 3A). One-way ANOVA was used to analyse all other data. In all cases, *post-hoc* analyses relied on Bonferroni's multiple comparison test (GRAPHPAD PRISM v3.01). We used the Pearson product-moment correlation coefficient to measure the strength of the linear relationship between the number of plaque-associated p-p38(MAPK)-IR cells and the plaque core size (GRAPHPAD PRISM v3.01) (Fig. 6). Stereological statistical sampling (Schmitz & Hof, 2005) is described in the section 'Stereological quantitative analysis' (above) and was performed using the STEREO INVESTIGATOR software (MicroBrightField, Inc.). Data are represented as mean ± SEM and P-values are provided as summary statistics.

Results

Fibrillar and non-fibrillar β-amyloid increases with age in the sensorimotor cortex of TgCRND8 mice

The amount of 6E10 immunoreactivity as well as the number of thioflavin-S-positive plaques increased in an age-dependent manner in the sensorimotor cortex of TgCRND8 mice (Fig. 1A). Both dense-core and diffuse plaques were detected in TgCRND8 mouse cortex. In dense-core plaques, thioflavin-S staining was surrounded by a halo of immunoreactivity for 6E10, whereas diffuse plaques were 6E10-IR, but negative for thioflavin-S (Fig. 1A). These data confirm the aggressive nature of the expressed $APP_{Swe/Ind}$ allele (Chishti *et al.*, 2001) and confirm the validity of the age range of the mice that we chose to include in this study.

An equidistant distribution pattern of p-p38(MAPK)-IR cells was observed in the parenchyma of WT as well as TgCRND8 mouse cortex at all ages studied (Fig. 1B). A population of p-p38(MAPK)-IR cells in these same sections was also localized to putative Aβ plaques in the older TgCRND8 mice. DAB immunohistochemistry in the absence of the primary, i.e. anti-p-p38(MAPK), antibody was devoid of any specific signal (Fig. 1B).

Distribution of p-p38(MAPK) immunoreactivity in sensorimotor cortex of wildtype and TgCRND8 animals

The p-p38(MAPK)-IR sections stained for both thionin and thioflavin-S revealed that the thionin staining of the centres of the plaque was

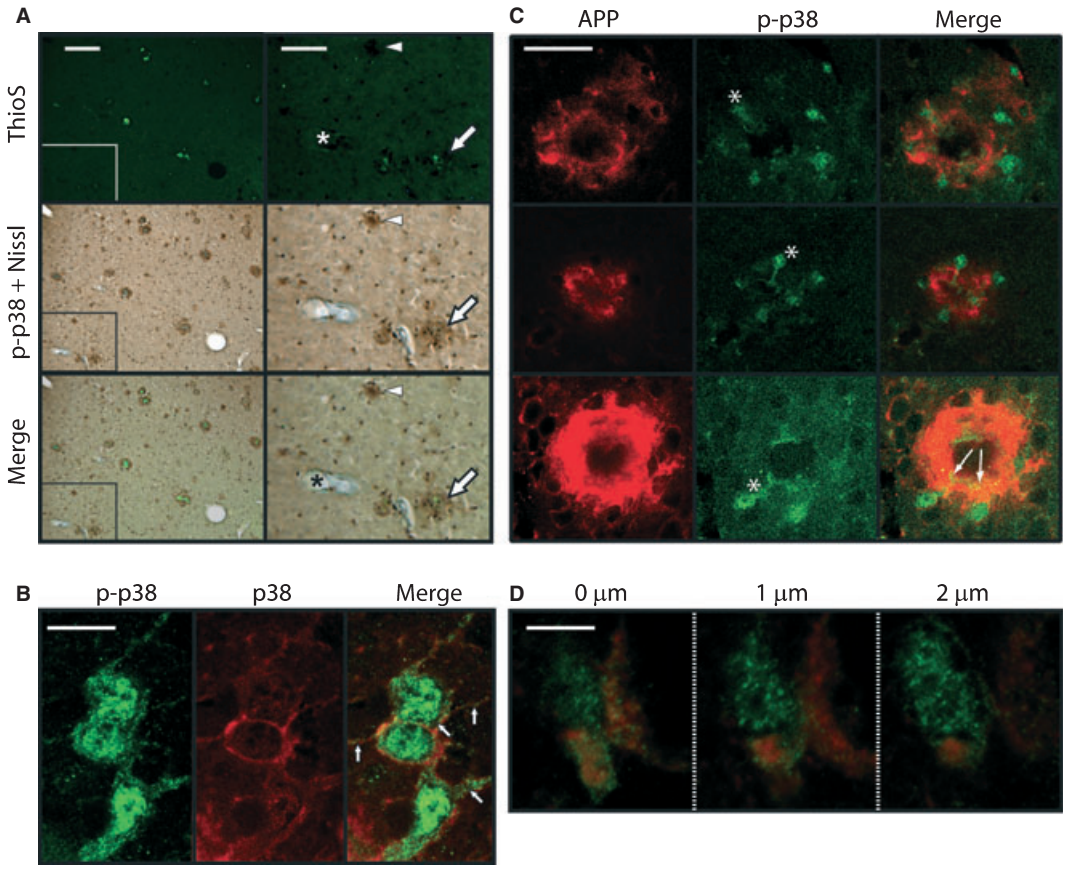

FIG. 2. p-p38(MAPK)-IR cells preferentially localize to dense-core plaques. (A) Left-hand panels; scale bar, 125 μm. A representative section of the sensorimotor cortex from a 10-month-old TgCRND8 mouse was stained with thioflavin-S (ThioS; top panel) and Nissl (blue; middle panel), and probed for p-p38(MAPK) immunoreactivity using DAB immunohistochemistry (middle panel). Note that the 'cores' of some plaques take up Nissl stain, appearing blue in colour. The merged panel (A, bottom) shows the co-localization of p-p38(MAPK), Nissl and thioflavin-S to some, but not all, Aβ plaques. (A) Right-hand panels; scale bar, 50 μm. Boxed areas from the left-hand panels were magnified. Arrows indicate a thioflavin-S-positive dense-core plaque, whereas the arrowhead indicates a putative diffuse plaque. Note that p-p38(MAPK)-IR cells localize to both types of plaque. Asterisk indicates a blood vessel. (B) Double-immunolabeling with anti-p38(MAPK) and anti-p-p38(MAPK) confirms that both antibodies label the same cells. Although there is overlap in the p38(MAPK)/p-p38(MAPK) signals, particularly in the processes (arrows), the p-p38(MAPK) signal is predominantly nuclear, as expected of p-p38(MAPK). (C) Laser-scanning confocal microscopy was used to confirm the localization of p-p38(MAPK) immunoreactivity to two separate APP/Aβ deposits (i.e. detected using the 6E10 anti-APP antibody, which does not differentiate between the precursor APP and the Aβ cleavage product). The radial distribution of p-p38(MAPK)-IR cells is clear in both images as is the observation that the immediate areas around the p-p38(MAPK)-IR cells are devoid of 6E10 immunoreactivity. These images also reveal that p-p38(MAPK)-IR cells do not simply surround the plaques, but that their processes can extend in a spoke-like fashion (indicated by asterisks) well into the area of the plaque. The merged signal (C, bottom panels, arrows) suggests that the 6E10 signal is intracellular (phagocytosed). (D) Three confocal images collected along the *z*-axis (*z*-stack; at 1 μm intervals) of a p-p38(MAPK)-IR cell (green) in which a 6E10 signal (red) is clearly evident. The p-p38(MAPK)-IR cell in these images is adjacent to a crescent-shaped 6E10-positive deposit. Scale bar – B, 5 μm; C, 10 μm; D, 3 μm.

paralleled by staining for thioflavin-S (Fig. 2A). p-p38(MAPK)-IR cells were also observed in clusters that were Aβ/6E10-positive, but that were not associated with thioflavin-S or thionin staining. Thus, p-p38(MAPK)-IR cell clusters were associated with both dense-core and diffuse plaques. Several vasculature-associated p-p38(MAPK)-IR cells were also observed (asterisk in Fig. 2A). As expected, p-p38(MAPK)-IR cells were also immunoreactive for p38(MAPK) (Fig. 2B). The p-p38(MAPK) and p38(MAPK) signals co-localized particularly in cell processes but, as shown previously (Wood *et al.*, 2009), most of the activated form, i.e. p-p38(MAPK), was nuclear. Confocal microscopy confirmed the integration of p-p38(MAPK)-IR cells to 6E10-IR aggregates (Fig. 2C). In these dense-core plaques, the bodies of p-p38(MAPK)-IR cells localized to the outer 6E10-IR penumbra of the amyloid plaque rather than within the thioflavin-S-positive aspect of the amyloid core. However, the processes of these same cells extended through the 6E10-IR penumbra and usually ended just within the border of the thioflavin-S-stained amyloid core. In some cases, the 6E10 signal was co-detected with the p-p38(MAPK) signal, suggesting that Aβ was being taken into the cell (phagocytosed; Fig. 2C, bottom panels). The latter is supported by images collected from a series of focal planes (separated by 1 μm steps), representing digital serial sections (Z-stack), and clearly showing a 6E10-positive signal within the p-p38(MAPK) signal (Fig. 2D). These combined data provide the first evidence for the association of p-p38(MAPK)-IR cells with Aβ deposits in the TgCRND8 mouse sensorimotor cortex. We next chose to determine whether there was a particular type of plaque, i.e. diffuse vs. dense-core, to which these cells were localizing.

Quantification and distribution of p-p38(MAPK)-immunoreactive cells in sensorimotor cortex of TgCRND8 mice

The p-p38(MAPK)-IR MCCs obtained by stereological sampling were subjected to a two-way ANOVA based on two genotypes (WT and TgCRND8) and three ages (3, 6 and 10 months). Three analyses were

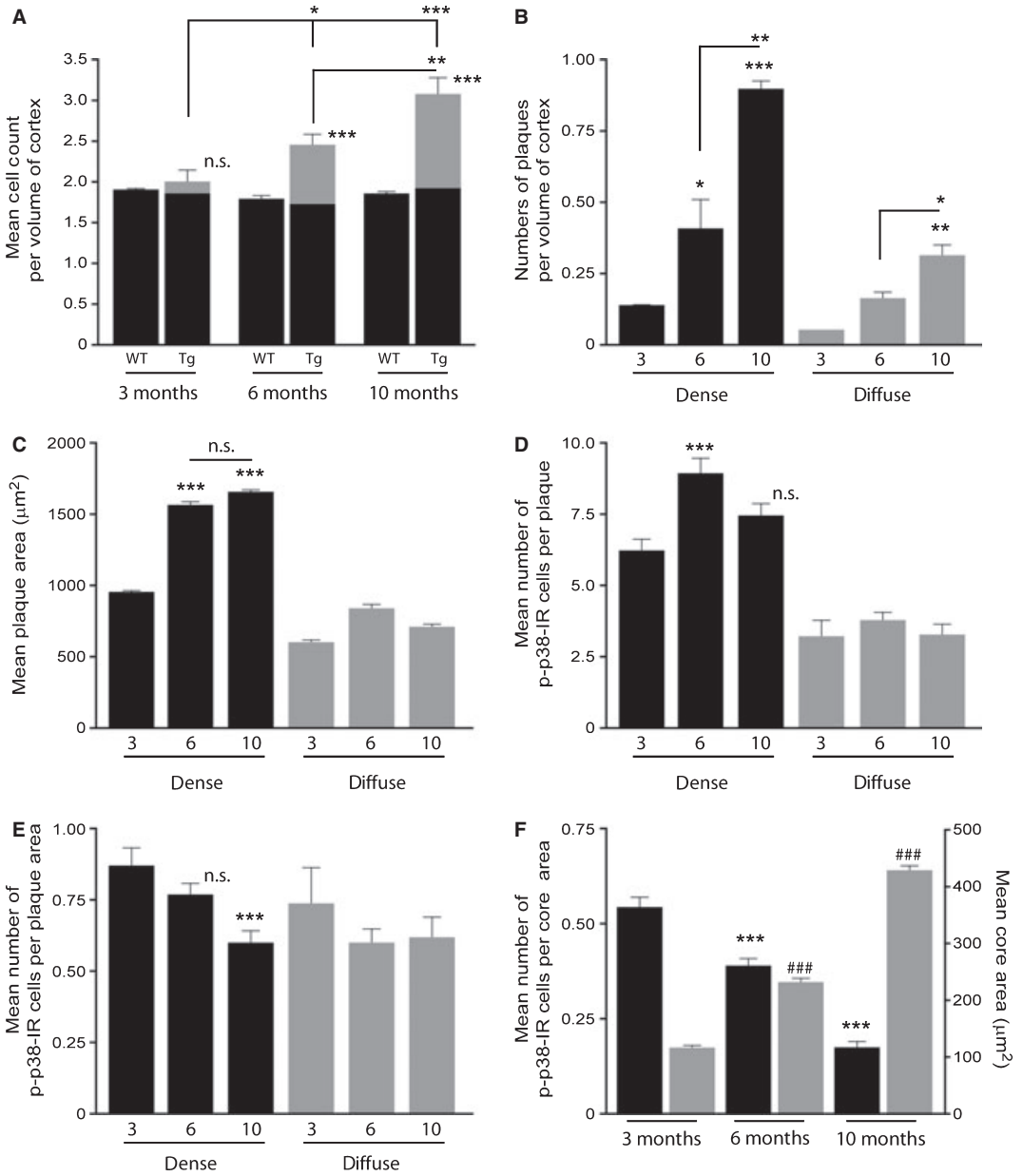

FIG. 3. Quantification of parenchymal- and plaque-associated p-p38(MAPK)-IR cells. (A) p-p38(MAPK)-IR cells in WT and TgCRND8 (Tg) mouse cortex were quantified using stereological sampling and categorized as parenchymal (not in the vicinity of a plaque; black bars) and plaque-associated (in physical contact with a plaque; grey bars). The age-dependent increase in the density (number of cells per volume of cortex) of p-p38(MAPK)-IR cells was exclusively in the plaque-associated pool of cells. (B) The number of dense-core (dense) and diffuse plaques (per volume of cortex) increases with age. (C) The average area of dense-core plaques increases with age, whereas that of diffuse plaques does not. (D) The mean number of p-p38(MAPK)-IR cells per individual dense-core plaque (but not diffuse plaques) increases by 6 months of age, but is no longer significantly different from 3-month-old mouse cortex by 10 months of age. (E) However, larger dense-core plaques have a lower relative number of p-p38(MAPK)-IR cells. (F) There is an inverse relation between the size of a dense core within a given plaque (grey bars) and the number of p-p38(MAPK)-IR cells associated with the plaque (black bars). 3, 6 and 10 indicate 3-, 6- and 10-month-old, respectively. n = 3–4 animals; *$P < 0.05$; **$P < 0.01$; ***$P < 0.001$ vs. respective controls or between indicated groups. $^{###}P < 0.001$ vs. core area in 3-month-old controls. n.s., not significant.

performed: (i) using the total MCC; and subsequently dividing the total MCC into (ii) plaque-associated MCC and (iii) parenchymal MCC. In the case of total MCC, both genotype ($F_{1,12} = 89.8$, $P < 0.0001$) and age ($F_{2,12} = 16.97$, $P = 0.0003$) exerted an effect. The interaction was also significant ($F_{2,12} = 19.46$, $P = 0.0002$), indicating that the changes in MCC were dependent on both genotype and age (Fig. 3A). Analysis based on the plaque-associated MCC also revealed a significant effect of genotype ($F_{1,12} = 184.2$, $P < 0.0001$) and age ($F_{2,12} = 36.35$, $P < 0.0001$), and a significant interaction ($F_{2,12} = 36.35$, $P < 0.0001$). In contrast, analysis based on parenchymal MCC revealed a non-significant effect of genotype ($F_{1,12} = 0.0990$, $P = 0.7584$) and a modest effect of age ($F_{2,12} = 5.517$, $P = 0.02$). The interaction effect was non-significant ($F_{2,12} = 0.5538$, $P = 0.5888$). The effect seen with total MCC therefore reflected the changes in genotype- and age-dependent plaque-associated p-p38(MAPK)-IR MCC (Fig. 3A).

Non-stereological semi-quantitative estimates confirmed the age-dependent increase in the density (number of plaques per volume) of

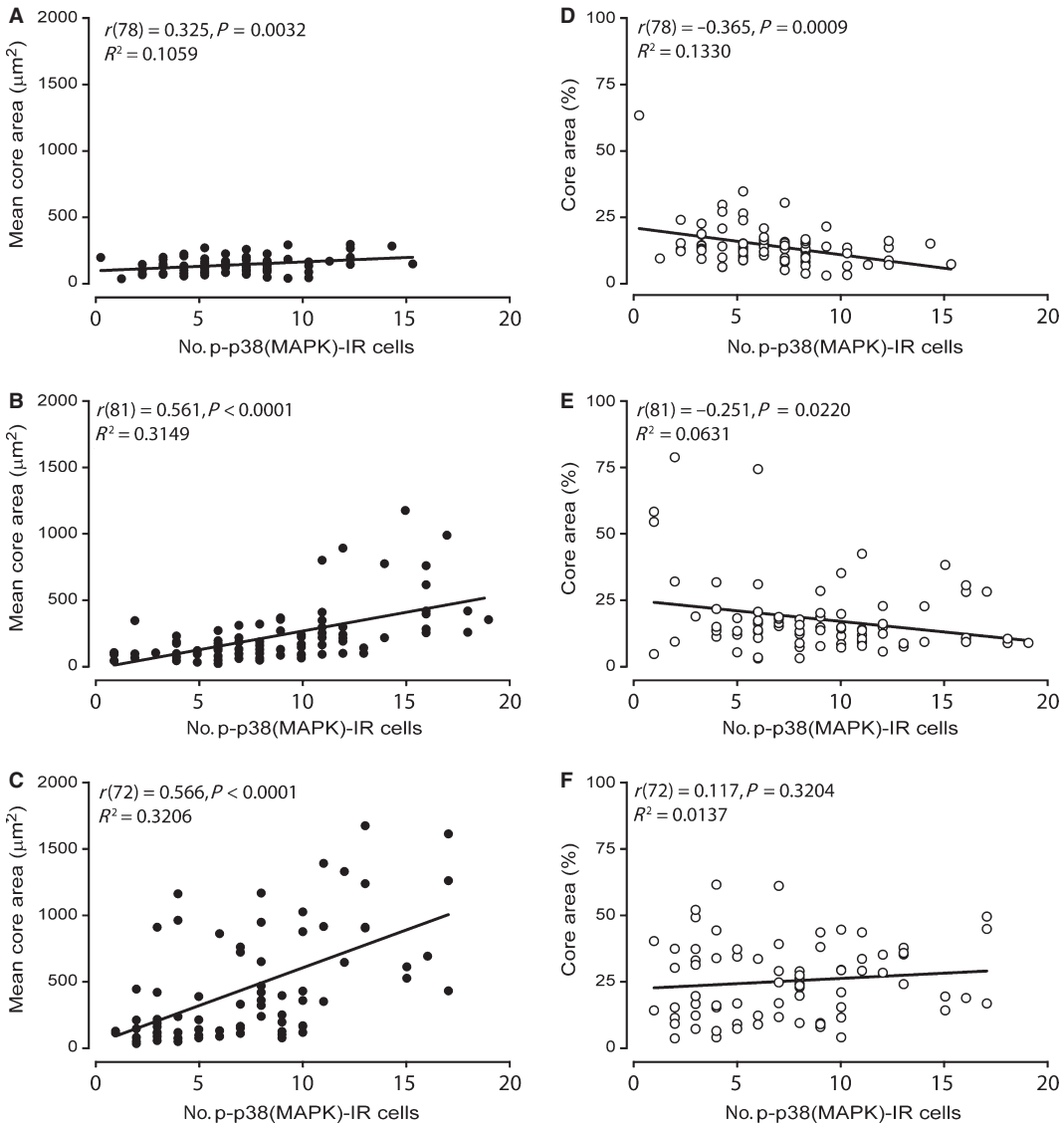

FIG. 4. There is an inverse correlation between dense-core plaque-associated p-p38(MAPK)-IR cells and core size. The number of p-p38(MAPK)-IR cells around a given plaque in the cortex of (A and D) 3-month-old, (B and E) 6-month-old and (C and F) 10-month-old TgCRND8 mice were expressed either (A–C) as a function of the absolute size (in μm^2) of the core within the given plaque or (D–F) as a function of the ratio of the core size to that of the plaque within which it resides (i.e. plaques with larger cores score higher on the *Y*-axis). Correlation coefficients (Pearson's *r*-values), statistical summary and the coefficient of linear regression (R^2) are included with each dataset. Cell counts are derived from four to five animals per group.

cortical plaques (see Fig. 1). The increase was predominantly associated with dense-core plaques ($F_{2,6} = 44.68$, $P = 0.0002$), although the density of diffuse plaques also increased, albeit more modestly ($F_{2,6} = 20.85$, $P = 0.0020$; Fig. 3B). The size (area) of individual dense-core plaques increased with age ($F_{2,234} = 12.17$, $P < 0.0001$), whereas the size of diffuse plaques did not increase significantly beyond the size that was already present in 3-month-old TgCRND8 mice ($F_{2,91} = 1.561$, $P = 0.2155$; Fig. 3C). The number of p-p38(MAPK)-IR cells per diffuse plaque remained unchanged with age ($F_{2,91} = 0.6351$, $P = 0.5322$; Fig. 3D), whereas the number of p-p38(MAPK)-IR cells localizing to individual dense-core plaques increased in the 6-month-old TgCRND8 mice ($F_{2,234} = 9.513$, $P < 0.0001$; although the latter effect was no longer significant in the 10-month-old mice – Fig. 3D). This was somewhat perplexing as one would have assumed, at the very least, a maintenance of p-p38(MAPK)-IR residency in the area of dense-core plaques. Further examination revealed an age-dependent decrease in the mean number of p-p38(MAPK)-IR cells as a function of dense-core plaque size ($F_{2,234} = 10.92$, $P < 0.0001$; Fig. 3E). Once again, there was no effect associated with diffuse plaques ($F_{2,91} = 0.7643$, $P = 0.4686$) (Fig. 3E). The relevance of the age-dependent decrease in p-p38(MAPK)-IR cells as a function of dense-core plaque area (observed in Fig. 3E, above) was underscored by the subsequent observation that, although the average size of individual thioflavin-S-positive cores increased with age ($F_{2,234} = 19.52$, $P < 0.0001$), the mean number of p-p38(MAPK)-IR cells associated with these same thioflavin-S-positive cores was decreased ($F_{2,234} = 70.16$, $P < 0.0001$; Fig. 3F). These data suggest that the growth of a dense-core plaque will plateau with age, but that the size of the thioflavin-S-positive Aβ conformation at its core will continue to develop and that this core development is inversely correlated with the number of plaque-associated p-p38(MAPK)-IR cells.

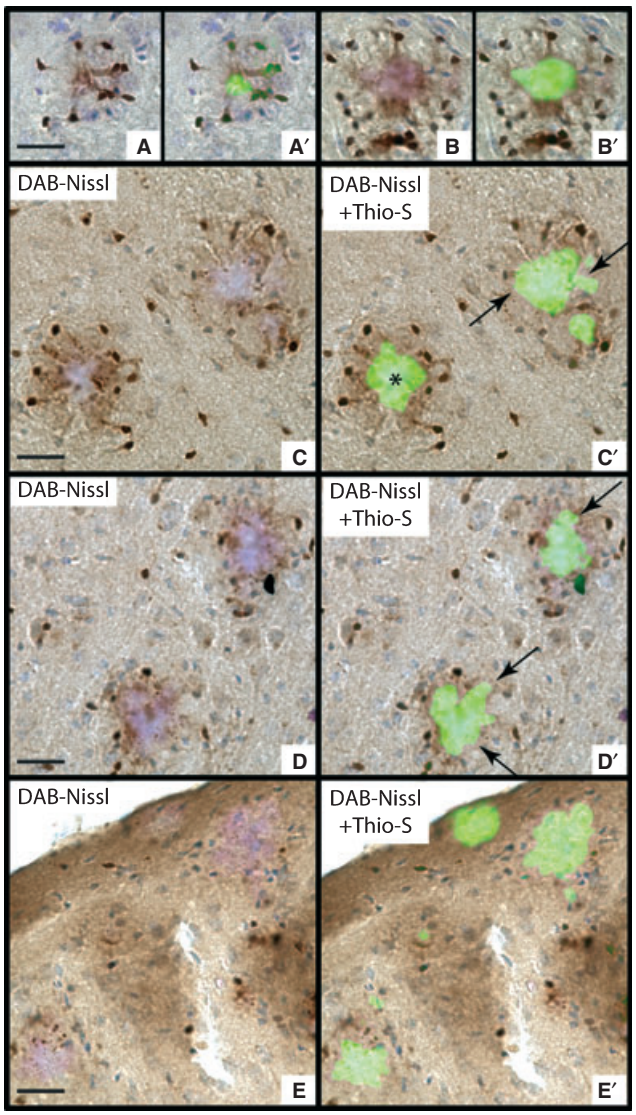

FIG. 5. The loss of p-p38(MAPK)-IR cells around a plaque coincides with expansion of thioflavin-S staining. Sections were probed for p-p38(MAPK) using DAB immunohistochemistry and stained for thionin/Nissl (purple) and counterstained for thioflavin-S (green). The DAB–Nissl sections (i.e. A–E) clearly show the distribution of p-p38(MAPK)-IR cells around putative plaques. The thionin stain detects Nissl substance in individual cells as well as in the core of these plaques. The corresponding thioflavin-S (green) stained series (i.e. A′–E′) clearly identifies these same thionin-stained cores. (A, A′, B and B′) The radial/circumferential distribution of p-p38(MAPK)-IR cells around plaques is evident as are the spoke-like extensions invading the plaque (as observed using confocal microscopy, see Fig. 2). (C, C′, D and D′) The loss of p-p38(MAPK)-IR cells in the vicinity of a plaque allows for the Nissl/thioflavin-S core to expand uncontrollably (arrows). Asterisk indicates a 'restricted' core within a plaque with circumferential distribution of p-p38(MAPK)-IR cells. (E and E′) Superficial layers of the cortex contain patches that are identified by thionin/Nissl staining and subsequently confirmed to be dense-core plaques by thioflavin-S staining. There are no p-p38(MAPK)-IR cells associated with these amorphic plaques. Scale bar – A–D and A′–D′, 20 μm; E and E′, 25 μm.

The correlation of p-p38(MAPK)-immunoreactive cell density differs with absolute vs. proportional core size

We next evaluated the linear relation between p-p38(MAPK)-IR cells and core size using Pearson's correlation. We expressed the mean number of p-p38(MAPK)-IR cells as a function of either absolute core size (i.e. in μm^2) or a function of relative core size (i.e. percentage of total plaque area that is occupied by the core). We found that there was a positive correlation between the mean number of p-p38(MAPK)-IR cells and absolute core size, and that this correlation was enhanced as a function of age (Fig. 4, left-hand panels; statistics included in the respective panels). However, if the area of a given core was expressed as a function of its area-occupancy within a given plaque, then the opposite relation held, i.e. there was a negative correlation between the mean number of p-p38(MAPK)-IR cells and proportional core size, and this was lost as a function of age (Fig. 4, right-hand panels; statistics included in the respective panels).

The dense core of a plaque expands along the aspect that is devoid of p-p38(MAPK)-immunoreactive cells

Examples of the radial/circumferential distribution of p-p38 (MAPK)-IR cells around dense-core (i.e. thioflavin-S-positive) plaques are presented in Fig. 5A, A′ and B, B′. Thionin staining clearly detects Nissl substance in thioflavin-S-positive plaques. In Fig. 5C, C′ and D, D′, we provide evidence of a 'restricted' core, i.e. one within a plaque with radially distributed p-p38(MAPK)-IR cells, as well as cores that are expanding amorphously. In these latter plaques, the cores tend to expand outward along the aspect of the plaque where p-p38(MAPK)-IR cells are no longer present. In Fig. 5E and E′, uncontrolled growth and amorphic dense-core plaques devoid of any associated p-p38(MAPK)-IR cells are clearly evident in the superficial layers of the cortex. In these areas, putative plaques are initially identified by Nissl staining and subsequently confirmed by staining with thioflavin-S.

These data strongly suggest that p-p38(MAPK)-IR cells play a greater role in restricting thioflavin-S-positive core maturation than in accumulating Aβ into aggregate/plaques, and that this interference in core maturation diminishes with age. Our final objective was to determine the phenotype of the sampled p-p38(MAPK)-IR cell population.

Identification of p-p38(MAPK)-immunoreactive cells by double immunofluorescence

Others (Giovannini *et al.*, 2008) have immunodetected p-p38(MAPK) in activated astrocytes (GFAP-positive) and microglia [major histocompatibility complex (MHC) II-positive] as well as in neurons (NeuN-positive) of the hippocampus of TgCRND8 mice. In contrast, in the sensorimotor cortex of TgCRND8 mice, p-p38(MAPK) was occasionally detected in neuronal cell bodies (NeuN) and rarely in GFAP-positive astrocytes (Fig. 6A and C). Although there was evidence of some plaque-associated p-p38(MAPK)-IR cells expressing the ED-1 (CD68) monocytic marker (Fig. 6B and D), the vast majority of p-p38(MAPK)-IR cells associated with either the parenchyma (of both WT and TgCRND8 mice) or 6E10-positive plaques were also labelled with the microglial marker Mac-1 (Fig. 6B, D and E). The Mac-1 antibody, as expected, labelled the plasma membrane; in these same cells the p-p38(MAPK) signal was evident in the cytoplasm and its processes. We observed that the intensity of Mac-1 immunoreactivity was most evident around plaques in the cortex of the 10-month-old TgCRND8 mice (Fig. 6D and E).

These data confirm that p38(MAPK) is constitutively phosphorylated in a population of cortical microglia regardless of genotype, and that a population of p-p38(MAPK)-IR, Mac-1-positive micro-

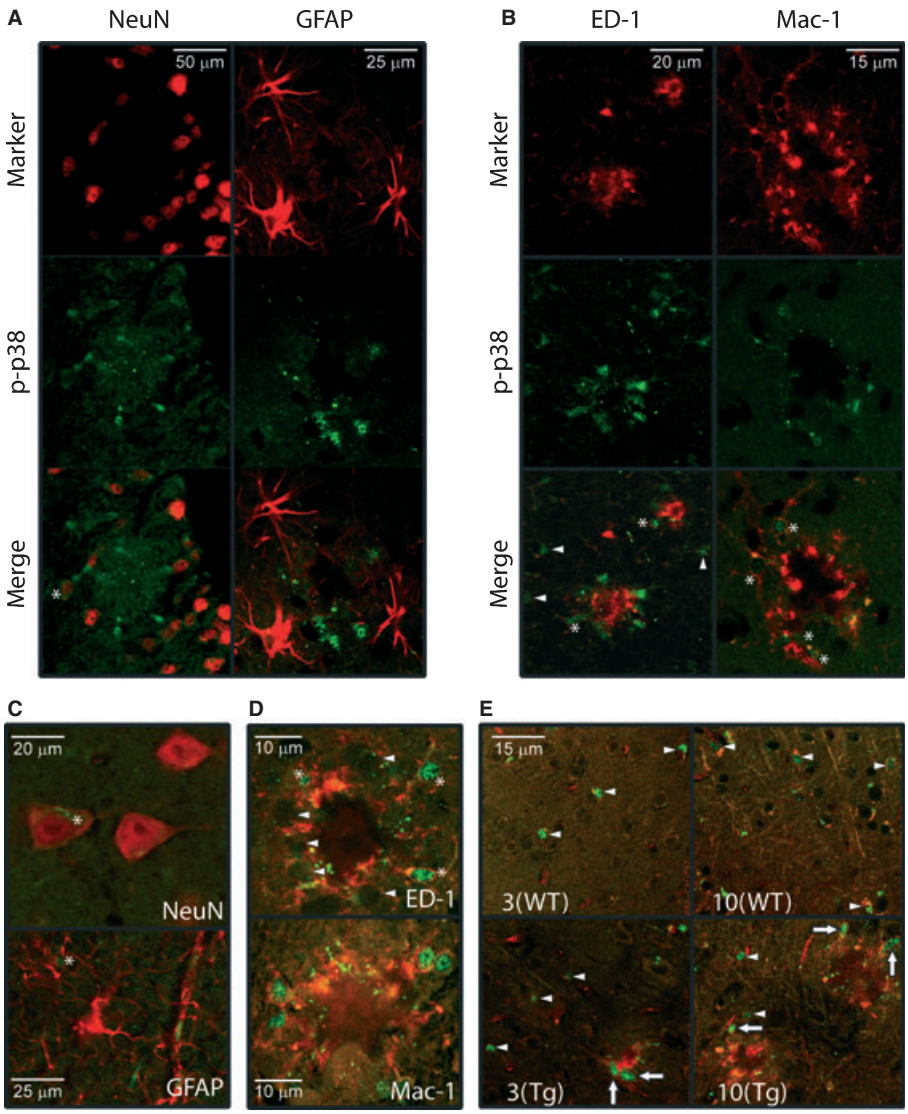

FIG. 6. Plaque-associated p-p38(MAPK)-IR cells are primarily Mac-1-positive microglia. (A) Sections were probed for p-p38(MAPK) immunoreactivity (green in all cases) and for NeuN (neurons) or GFAP (astrocytes). p-p38(MAPK) was detected in the occasional NeuN-positive cells (A and C; asterisks) and very rarely in GFAP-positive cells (C; asterisks). (B) Parenchymal p-p38(MAPK)-IR cells express an almost negligible ectodermal dysplasia-1 (CD68) (ED-1) signal (B; arrowheads), whereas p-p38(MAPK) immunoreactivity is detected, albeit infrequently, in plaque-associated ED-1-positive cells (monocytes/microglia) (B and D; asterisks). Many plaque-associated ED-1-IR cells are not immunoreactive for p-p38(MAPK) (D; arrowheads). In contrast, plaque-associated p-p38(MAPK)-IR cells clearly also express the Mac-1 (monocytes/microglia) marker [B (asterisks) and D]. (E) p-p38(MAPK) immunoreactivity is detected in parenchymal cells with a weak Mac-1 signal (arrowheads). The Mac-1 signal is weakest in 3-month-old WT [3(WT)] cortical field and strongest in the 10-month-old transgenic mouse cortical field. Plaque-associated p-p38(MAPK)-IR cells (arrows) have the strongest Mac-1 signal. 3(WT)/10(WT), 3- and 10-month-old WT; 3(Tg)/10(Tg), 3- and 10-month-old TgCRND8.

glia localize to the vicinity of plaques in the TgCRND8 mouse model of AD-related amyloidosis. The purpose of these p-p38(MAPK)-IR microglia appears to involve interference in core development.

Discussion

The dense-core amyloid plaque is inflammatory and, consequently, recruits microglia and astrocytes during AD (D'Andrea & Nagele, 2009). p38(MAPK) signalling is often enhanced near these plaques (Koistinaho *et al.*, 2002; Puig *et al.*, 2004) and, although cell-dependent p38(MAPK) signalling could be detrimental in AD (Hensley *et al.*, 1999; Pei *et al.*, 2001; Savage *et al.*, 2002; Bellucci *et al.*, 2007), the recruitment of microglia [many of which are p-p38(MAPK)-IR (Giovannini *et al.*, 2008)] to the vicinity of plaques could be exerting beneficial effects via mitigation of the Aβ burden and plaque development (Simard *et al.*, 2006; El Khoury *et al.*, 2007; Grathwohl *et al.*, 2009).

Changes in the function of the sensorimotor cortex predispose to cognitive impairment during normal ageing (Yakushev *et al.*, 2009) and particularly during AD progression (Frisoni *et al.*, 2009). p-p38(MAPK)-IR cells in the sensorimotor cortex of the TgCRND8 mouse are predominantly Mac-1-IR microglia (current study), although we did occasionally detect p-p38(MAPK)-IR neurons and, only very rarely, astrocytes. This cell-type-specific distribution of p-p38(MAPK) immunoreactivity generally concurs with previous reports using animal models of AD (Koistinaho *et al.*, 2002; Bellucci

et al., 2007; Giovannini *et al.*, 2008), and reflects observations made in other *in vivo* models, e.g. of spinal cord injury (Jin *et al.*, 2003; Yune *et al.*, 2007) and hypoxia (Bu *et al.*, 2007).

The presence of p38(MAPK)-immunoreactive microglia across the cortical mantle in both wildtype and TgCRND8 animals suggests a non-pathological role for these cells

Plaque-associated p-p38(MAPK)-IR microglia (Koistinaho *et al.*, 2002; Puig *et al.*, 2004) are thought to indicate localized detrimental inflammatory mechanisms during the course of AD (Culbert *et al.*, 2006). Previous reports have also indicated an increase, and activation, in a parenchymal pool of p-p38(MAPK)-IR cells in TgCRND8 mice (Koistinaho *et al.*, 2002; Giovannini *et al.*, 2008). Although we were able to confirm a parenchymal pool of p-p38(MAPK)-IR cells, our analyses also revealed that these cells were uniformly distributed and were positive for constitutively p-p38(MAPK) in both WT and TgCRND8 cortices, and that they did not change as a function of either genotype or age. What was particularly evident with these parenchymal p-p38(MAPK)-IR microglia was that even those microglia in the immediate vicinity of, but not in contact with, senile plaques had ramified processes typical of a 'resting' morphology (Nimmerjahn *et al.*, 2005; Hua & Walz, 2006; Bolmont *et al.*, 2008), and appeared to be largely unaffected by the microglial response at the neighbouring dense-core plaque. This was the case even in older TgCRND8 animals, when plaque deposition across the cortical mantle was significant and there were substantially more p-p38(MAPK)-IR cells around senile plaques. This constitutive p-p38(MAPK)-IR/resting microglial population strongly suggests a role for p38(MAPK) signalling in the ongoing, homeostatic maintenance of the brain parenchyma (rather than activation in response to plaque formation). Physiologically beneficial, constitutively activated p38(MAPK)-IR cells exist in several brain regions, including the cortex, hippocampus and cerebellum (Lee *et al.*, 2000).

The density of plaque-associated p-p38(MAPK)-immunoreactive microglia is inversely related to the size of thioflavin-S-positive amyloid cores

Both dense-core and diffuse plaques were clearly evident in TgCRND8 mouse cortex, yet statistical sampling indicated that p-p38(MAPK)-IR cells were most often detected in the vicinity of dense-core plaques (e.g. Fig. 3D). Furthermore, dense-core plaques with a uniform radial or circumferential distribution of p-p38(MAPK)-IR cells tended to have smaller core sizes. Our data cannot confirm that the increased presence of p-p38(MAPK)-IR cells around senile plaques is causally related to proportionately smaller, thioflavin-S-positive cores. However, it was evident that larger, more amorphous thioflavin-S-positive plaques were associated with fewer p-p38(MAPK)-IR cells, particularly in the older transgenic mice and in the superficial layers of the cortex (see Fig. 5E and E′), and that the expansion of these plaques inevitably occurred along aspects of the plaque's periphery that were devoid of p-p38(MAPK)-IR cells. Interestingly, the leading edge of the thioflavin-S stain in smaller-cored plaques often overlapped with the terminals of processes radiating inward from the surrounding microglia. Although we were able to detect a co-localized signal for Aβ (i.e. 6E10) and p-p38(MAPK) (see Fig. 2C and D) that suggests phagocytosis of Aβ, it is unclear whether these microglia simply clear non-fibrillar Aβ or whether these cells actually denature and remove fibrillar Aβ from the plaque core. Regardless, our findings corroborate those of others who have shown that induction of plaque-associated microglial cells restricts the development of dense-core plaques (Boissonneault *et al.*, 2009), whereas inhibition of microglial p38(MAPK) prevents the phagocytosis of fibrillar Aβ (Reed-Geaghan *et al.*, 2009).

Parenthetically, we observed Mac-1 immunoreactivity in the membranes of both parenchymal and plaque-associated p-p38(MAPK)-IR cells and, although not quantified, observed that the intensity of Mac-1 immunoreactivity increased only in plaque-associated p-p38(MAPK)-IR cells. We believe this observation to be significant as the Mac-1 antibody recognizes the complement C3 receptor, which, if deficient, is known to predispose to accelerated amyloid plaque deposition in transgenic mice (Maier *et al.*, 2008), and, if activated, facilitates the phagocytosis and clearance of Aβ (Choucair-Jaafar *et al.*, 2011).

Functions and origins of parenchymal vs. plaque-associated p-p38(MAPK)-immunoreactive microglia

Given that the density of plaque-associated, but not parenchymal, p-p38(MAPK)-IR cells increases with Aβ burden, this begs the question as to whether these two seemingly 'different' populations of p-p38(MAPK)-IR microglia have differential origins and functions in the response to Aβ. We cannot tell if the p-p38(MAPK) microglia surrounding the senile plaques originated solely from the brain parenchyma, if they were blood born/bone-marrow derived (Simard *et al.*, 2006; El Khoury *et al.*, 2007; Malm *et al.*, 2010), if they were mitotically derived locally from either population (Bornemann *et al.*, 2001), or if they were derived from some other unknown source. Frautschy's group has reported a measurable loss of microglial density as a function of distance from the plaque core in the Tg2576 mouse model of AD-related amyloidosis (Frautschy *et al.*, 1998), suggesting recruitment from the immediate parenchymal cell population. Given that the distribution and resting morphology of parenchymal p-p38(MAPK)-IR cells was not disrupted even in the 10-month-old TgCRND8 mouse cortex, these combined observations suggest that some of the p-p38(MAPK)-IR microglia surrounding senile plaques might be recruited from sources other than the brain parenchyma. Not surprisingly, and as reported elsewhere (Simard *et al.*, 2006; D'Andrea & Nagele, 2009), we detected several p-p38(MAPK)-IR cells within blood vessels, suggesting that at least some of the plaque-associated p-p38(MAPK)-IR microglia may have originated from the peripheral vasculature. Given the report of 5-bromo-2′-deoxyuridine (BrdU)-positive microglia surrounding dense-core plaques (Bornemann *et al.*, 2001), it is also possible that local mitosis of p-p38(MAPK)-positive microglia may be another source of these plaque-associated microglia.

Our observed differences in the morphologies of parenchymal and plaque-associated p-p38(MAPK)-IR cells in the TgCRND8 mouse cortex (which were of 'resting' and activated morphology, respectively) suggest that these two populations have different functions. Others have shown that so-called 'resting' microglia are continuously extending and retracting their processes so as to 'sample' the extracellular environment (Davalos *et al.*, 2005). In the context of AD, it is thought that only a limited number of 'resting' or parenchymal microglia are involved in the initial response to Aβ, and that bone marrow-derived cells (probably of macrophage lineage) (El Khoury *et al.*, 2007; Malm *et al.*, 2010) will be recruited from the periphery and transformed into microglia (Simard & Rivest, 2004). This would occur only after resident microglia have detected Aβ and released the necessary chemotaxic factors into the circulation. These newly transformed microglia have different inherent properties, e.g. a

more acidic lysosomal compartment and different phagocytotic properties, which render them more efficient than the intrinsic microglia at eliminating Aβ (Majumdar *et al.*, 2007). The role of bone marrow-derived microglia in restricting dense-core plaque development is supported by the finding that the *in vivo* ablation of microglial/macrophage cells in several animal models of AD reduces the number of plaque-associated microglia and promotes the growth of dense-core plaques (Simard *et al.*, 2006; Bolmont *et al.*, 2008). Thus, as we have shown that the morphology, distribution and density of the parenchymal p-p38(MAPK)-IR cells remain constant regardless of the age, genotype or degree of Aβ deposition, we would suggest that parenchymal p-p38(MAPK)-IR cells may play a role in the normal, ongoing homeostatic maintenance of the parenchymal environment, and that with increasing Aβ burden, p-p38(MAPK)-IR microglia cells must be recruited from the periphery in order to effectively restrict the growth of dense-core plaques.

Concluding remarks

Our combined data are the first to use stereological methods to examine the distribution of p-p38(MAPK)-IR cells in a mouse model of AD-related pathology. Our analyses reveal that the size of the thioflavin-S-positive (fibrillar) Aβ conformation that forms the 'dense core' will continue to develop with age, and that this core development is inversely correlated with the number of p-p38(MAPK)-IR microglia in the immediate vicinity of the plaque. This strongly suggests that, with age, the decreasing availability of p-p38(MAPK)-IR microglia may be related to the increasing fibrillar Aβ load.

The literature is now very clear that activated microglia localize to senile plaques. In the acute phase, microglia phagocytose and degrade Aβ. However, with a chronic insult, the continued activation of microglia inevitably causes release of chemokines and damaging cytokines. These phase-dependent roles of microglia and p38(MAPK) need to be duly considered when discussing the role of cell signalling, and particularly inflammation- or stress-associated signalling events, in the context of both experimental and clinical AD.

Acknowledgements and Financial Disclosures

We are grateful for the technical assistance provided by Lewei Rui and Gloria Hooshmand. This work was funded by a departmental Alfred E. Molstad Trust Award (to T.Z.) and by a CIHR-Saskatchewan Health Research Foundation (SHRF) Operating Grant (to D.D.M.). D.D.M. holds the Saskatchewan Research Chair in Alzheimer's Disease and Related Dementias funded jointly by the Alzheimer Society of Saskatchewan and the SHRF. There are no competing interests.

Abbreviations

Aβ, β-amyloid; AD, Alzheimer's disease; APP, amyloid-β protein precursor; BrDu, 5-bromo-2′-deoxyuridine; DAB, 3,3′-diaminobenzidine; ED-1, ectodermal dysplasia-1 (CD68); GFAP, glial fibrillary acidic protein; IR, immunoreactive; Mac-1, Macrophage-1 (CD11b/CD18); MCC, mean cell count; MHC, major histocompatibility complex; NeuN, neuronal-specific antibody; p38(MAPK), p38 mitogen-activated protein kinase; PBS, phosphate-buffered saline; p-p38(MAPK), phosphorylated p38 mitogen-activated protein kinase; RT, room temperature; WT, wildtype.

References

Bellucci, A., Rosi, M.C., Grossi, C., Fiorentini, A., Luccarini, I. & Casamenti, F. (2007) Abnormal processing of tau in the brain of aged TgCRND8 mice. *Neurobiol. Dis.*, **27**, 328–338.

Boissonneault, V., Filali, M., Lessard, M., Relton, J., Wong, G. & Rivest, S. (2009) Powerful beneficial effects of macrophage colony-stimulating factor on beta-amyloid deposition and cognitive impairment in Alzheimer's disease. *Brain*, **132**, 1078–1092.

Bolmont, T., Haiss, F., Eicke, D., Radde, R., Mathis, C.A., Klunk, W.E., Kohsaka, S., Jucker, M. & Calhoun, M.E. (2008) Dynamics of the microglial/amyloid interaction indicate a role in plaque maintenance. *J. Neurosci.*, **28**, 4283–4292.

Bornemann, K.D., Wiederhold, K.H., Pauli, C., Ermini, F., Stalder, M., Schnell, L., Sommer, B., Jucker, M. & Staufenbiel, M. (2001) Abeta-induced inflammatory processes in microglia cells of APP23 transgenic mice. *Am. J. Pathol.*, **158**, 63–73.

Bu, X., Huang, P., Qi, Z., Zhang, N., Han, S., Fang, L. & Li, J. (2007) Cell type-specific activation of p38 MAPK in the brain regions of hypoxic preconditioned mice. *Neurochem. Int.*, **51**, 459–466.

Cao, X., Rui, L., Pennington, P.R., Chlan-Fourney, J., Jiang, Z., Wei, Z., Li, X.M., Edmondson, D.E. & Mousseau, D.D. (2009) Serine 209 resides within a putative p38(MAPK) consensus motif and regulates monoamine oxidase-A activity. *J. Neurochem.*, **111**, 101–110.

Chishti, M.A., Yang, D.S., Janus, C., Phinney, A.L., Horne, P., Pearson, J., Strome, R., Zuker, N., Loukides, J., French, J., Turner, S., Lozza, G., Grilli, M., Kunicki, S., Morissette, C., Paquette, J., Gervais, F., Bergeron, C., Fraser, P.E., Carlson, G.A., George-Hyslop, P.S. & Westaway, D. (2001) Early-onset amyloid deposition and cognitive deficits in transgenic mice expressing a double mutant form of amyloid precursor protein 695. *J. Biol. Chem.*, **276**, 21562–21570.

Choucair-Jaafar, N., Laporte, V., Levy, R., Poindron, P., Lombard, Y. & Gies, J.P. (2011) Complement receptor 3 (CD11b/CD18) is implicated in the elimination of beta-amyloid peptides. *Fundam. Clin. Pharmacol.*, **25**, 115–122.

Culbert, A.A., Skaper, S.D., Howlett, D.R., Evans, N.A., Facci, L., Soden, P.E., Seymour, Z.M., Guillot, F., Gaestel, M. & Richardson, J.C. (2006) MAPK-activated protein kinase 2 deficiency in microglia inhibits pro-inflammatory mediator release and resultant neurotoxicity. Relevance to neuroinflammation in a transgenic mouse model of Alzheimer disease. *J. Biol. Chem.*, **281**, 23658–23667.

D'Andrea, M.R. & Nagele, R.G. (2009) Morphologically distinct types of amyloid plaques point the way to a better understanding of Alzheimer's disease pathogenesis. *Biotech. Histochem.*, **85**, 133–147.

D'Andrea, M.R., Reiser, P.A., Gumula, N.A., Hertzog, B.M. & Andrade-Gordon, P. (2001) Application of triple immunohistochemistry to characterize amyloid plaque-associated inflammation in brains with Alzheimer's disease. *Biotech. Histochem.*, **76**, 97–106.

Davalos, D., Grutzendler, J., Yang, G., Kim, J.V., Zuo, Y., Jung, S., Littman, D.R., Dustin, M.L. & Gan, W.B. (2005) ATP mediates rapid microglial response to local brain injury in vivo. *Nat. Neurosci.*, **8**, 752–758.

El Khoury, J., Toft, M., Hickman, S.E., Means, T.K., Terada, K., Geula, C. & Luster, A.D. (2007) Ccr2 deficiency impairs microglial accumulation and accelerates progression of Alzheimer-like disease. *Nat. Med.*, **13**, 432–438.

Franklin, K. & Paxinos, G. (1997) *The Mouse Brain in Stereotaxic Coordinates*. Academic Press, San Diego.

Frautschy, S.A., Yang, F., Irrizarry, M., Hyman, B., Saido, T.C., Hsiao, K. & Cole, G.M. (1998) Microglial response to amyloid plaques in APPsw transgenic mice. *Am. J. Pathol.*, **152**, 307–317.

Frisoni, G.B., Prestia, A., Rasser, P.E., Bonetti, M. & Thompson, P.M. (2009) In vivo mapping of incremental cortical atrophy from incipient to overt Alzheimer's disease. *J. Neurol.*, **256**, 916–924.

Giovannini, M.G., Cerbai, F., Bellucci, A., Melani, C., Grossi, C., Bartolozzi, C., Nosi, D. & Casamenti, F. (2008) Differential activation of mitogen-activated protein kinase signalling pathways in the hippocampus of CRND8 transgenic mouse, a model of Alzheimer's disease. *Neuroscience*, **153**, 618–633.

Grathwohl, S.A., Kalin, R.E., Bolmont, T., Prokop, S., Winkelmann, G., Kaeser, S.A., Odenthal, J., Radde, R., Eldh, T., Gandy, S., Aguzzi, A., Staufenbiel, M., Mathews, P.M., Wolburg, H., Heppner, F.L. & Jucker, M. (2009) Formation and maintenance of Alzheimer's disease beta-amyloid plaques in the absence of microglia. *Nat. Neurosci.*, **12**, 1361–1363.

Hanisch, U.K. & Kettenmann, H. (2007) Microglia: active sensor and versatile effector cells in the normal and pathologic brain. *Nat. Neurosci.*, **10**, 1387–1394.

Hensley, K., Floyd, R.A., Zheng, N.Y., Nael, R., Robinson, K.A., Nguyen, X., Pye, Q.N., Stewart, C.A., Geddes, J., Markesbery, W.R., Patel, E., Johnson, G.V. & Bing, G. (1999) p38 kinase is activated in the Alzheimer's disease brain. *J. Neurochem.*, **72**, 2053–2058.

Honda, S., Sasaki, Y., Ohsawa, K., Imai, Y., Nakamura, Y., Inoue, K. & Kohsaka, S. (2001) Extracellular ATP or ADP induce chemotaxis of cultured microglia through Gi/o-coupled P2Y receptors. *J. Neurosci.*, **21**, 1975–1982.

Hua, R. & Walz, W. (2006) Minocycline treatment prevents cavitation in rats after a cortical devascularizing lesion. *Brain Res.*, **1090**, 172–181.

Jin, S.X., Zhuang, Z.Y., Woolf, C.J. & Ji, R.R. (2003) p38 mitogen-activated protein kinase is activated after a spinal nerve ligation in spinal cord microglia and dorsal root ganglion neurons and contributes to the generation of neuropathic pain. *J. Neurosci.*, **23**, 4017–4022.

Juretic, N., Santibanez, J.F., Hurtado, C. & Martinez, J. (2001) ERK 1,2 and p38 pathways are involved in the proliferative stimuli mediated by urokinase in osteoblastic SaOS-2 cell line. *J. Cell. Biochem.*, **83**, 92–98.

Koistinaho, M., Kettunen, M.I., Goldsteins, G., Keinanen, R., Salminen, A., Ort, M., Bures, J., Liu, D., Kauppinen, R.A., Higgins, L.S. & Koistinaho, J. (2002) Beta-amyloid precursor protein transgenic mice that harbor diffuse A beta deposits but do not form plaques show increased ischemic vulnerability: role of inflammation. *Proc. Natl Acad. Sci. USA*, **99**, 1610–1615.

Lee, S.H., Park, J., Che, Y., Han, P.L. & Lee, J.K. (2000) Constitutive activity and differential localization of p38alpha and p38beta MAPKs in adult mouse brain. *J. Neurosci. Res.*, **60**, 623–631.

Maier, M., Peng, Y., Jiang, L., Seabrook, T.J., Carroll, M.C. & Lemere, C.A. (2008) Complement C3 deficiency leads to accelerated amyloid beta plaque deposition and neurodegeneration and modulation of the microglia/macrophage phenotype in amyloid precursor protein transgenic mice. *J. Neurosci.*, **28**, 6333–6341.

Majumdar, A., Cruz, D., Asamoah, N., Buxbaum, A., Sohar, I., Lobel, P. & Maxfield, F.R. (2007) Activation of microglia acidifies lysosomes and leads to degradation of Alzheimer amyloid fibrils. *Mol. Biol. Cell*, **18**, 1490–1496.

Malm, T., Koistinaho, M., Muona, A., Magga, J. & Koistinaho, J. (2010) The role and therapeutic potential of monocytic cells in Alzheimer's disease. *Glia*, **58**, 889–900.

Morooka, T. & Nishida, E. (1998) Requirement of p38 mitogen-activated protein kinase for neuronal differentiation in PC12 cells. *J. Biol. Chem.*, **273**, 24285–24288.

Naderi, J., Lopez, C. & Pandey, S. (2006) Chronically increased oxidative stress in fibroblasts from Alzheimer's disease patients causes early senescence and renders resistance to apoptosis by oxidative stress. *Mech. Ageing Dev.*, **127**, 25–35.

Neary, J.T., Rathbone, M.P., Cattabeni, F., Abbracchio, M.P. & Burnstock, G. (1996) Trophic actions of extracellular nucleotides and nucleosides on glial and neuronal cells. *Trends Neurosci.*, **19**, 13–18.

Nimmerjahn, A., Kirchhoff, F. & Helmchen, F. (2005) Resting microglial cells are highly dynamic surveillants of brain parenchyma in vivo. *Science*, **308**, 1314–1318.

Park, J.G., Yuk, Y., Rhim, H., Yi, S.Y. & Yoo, Y.S. (2002) Role of p38 MAPK in the regulation of apoptosis signaling induced by TNF-alpha in differentiated PC12 cells. *J. Biochem. Mol. Biol.*, **35**, 267–272.

Pearson, R.C., Esiri, M.M., Hiorns, R.W., Wilcock, G.K. & Powell, T.P. (1985) Anatomical correlates of the distribution of the pathological changes in the neocortex in Alzheimer disease. *Proc. Natl Acad. Sci. USA*, **82**, 4531–4534.

Pei, J.J., Braak, E., Braak, H., Grundke-Iqbal, I., Iqbal, K., Winblad, B. & Cowburn, R.F. (2001) Localization of active forms of C-jun kinase (JNK) and p38 kinase in Alzheimer's disease brains at different stages of neurofibrillary degeneration. *J. Alzheimers Dis.*, **3**, 41–48.

Premkumar, D.R., Smith, M.A., Richey, P.L., Petersen, R.B., Castellani, R., Kutty, R.K., Wiggert, B., Perry, G. & Kalaria, R.N. (1995) Induction of heme oxygenase-1 mRNA and protein in neocortex and cerebral vessels in Alzheimer's disease. *J. Neurochem.*, **65**, 1399–1402.

Probst, A., Ulrich, J. & Heitz, P.U. (1982) Senile dementia of Alzheimer type: astroglial reaction to extracellular neurofibrillary tangles in the hippocampus. An immunocytochemical and electron-microscopic study. *Acta Neuropathol.*, **57**, 75–79.

Puig, B., Gomez-Isla, T., Ribe, E., Cuadrado, M., Torrejon-Escribano, B., Dalfo, E. & Ferrer, I. (2004) Expression of stress-activated kinases c-Jun N-terminal kinase (SAPK/JNK-P) and p38 kinase (p38-P), and tau hyperphosphorylation in neurites surrounding betaA plaques in APP Tg2576 mice. *Neuropathol. Appl. Neurobiol.*, **30**, 491–502.

Reed-Geaghan, E.G., Savage, J.C., Hise, A.G. & Landreth, G.E. (2009) CD14 and toll-like receptors 2 and 4 are required for fibrillar A{beta}-stimulated microglial activation. *J. Neurosci.*, **29**, 11982–11992.

Savage, M.J., Lin, Y.G., Ciallella, J.R., Flood, D.G. & Scott, R.W. (2002) Activation of c-Jun N-terminal kinase and p38 in an Alzheimer's disease model is associated with amyloid deposition. *J. Neurosci.*, **22**, 3376–3385.

Scheaffer, R.L., Mendenhall, W. & Ott, R.L. (1996) Systematic sampling (Ch. 7). *Elementary Survey Sampling*, 5th Edn. Duxbury Press, Boston.

Schmitz, C. & Hof, P.R. (2005) Design-based stereology in neuroscience. *Neuroscience*, **130**, 813–831.

Simard, A.R. & Rivest, S. (2004) Bone marrow stem cells have the ability to populate the entire central nervous system into fully differentiated parenchymal microglia. *FASEB J.*, **18**, 998–1000.

Simard, A.R., Soulet, D., Gowing, G., Julien, J.P. & Rivest, S. (2006) Bone marrow-derived microglia play a critical role in restricting senile plaque formation in Alzheimer's disease. *Neuron*, **49**, 489–502.

Stalder, M., Phinney, A., Probst, A., Sommer, B., Staufenbiel, M. & Jucker, M. (1999) Association of microglia with amyloid plaques in brains of APP23 transgenic mice. *Am. J. Pathol.*, **154**, 1673–1684.

Wada, T. & Penninger, J.M. (2004) Mitogen-activated protein kinases in apoptosis regulation. *Oncogene*, **23**, 2838–2849.

Wood, C.D., Thornton, T.M., Sabio, G., Davis, R.A. & Rincon, M. (2009) Nuclear localization of p38 MAPK in response to DNA damage. *Int. J. Biol. Sci.*, **5**, 428–437.

Yakushev, I., Hammers, A., Fellgiebel, A., Schmidtmann, I., Scheurich, A., Buchholz, H.G., Peters, J., Bartenstein, P., Lieb, K. & Schreckenberger, M. (2009) SPM-based count normalization provides excellent discrimination of mild Alzheimer's disease and amnestic mild cognitive impairment from healthy aging. *Neuroimage*, **44**, 43–50.

Yosimichi, G., Nakanishi, T., Nishida, T., Hattori, T., Takano-Yamamoto, T. & Takigawa, M. (2001) CTGF/Hcs24 induces chondrocyte differentiation through a p38 mitogen-activated protein kinase (p38MAPK), and proliferation through a p44/42 MAPK/extracellular-signal regulated kinase (ERK). *Eur. J. Biochem.*, **268**, 6058–6065.

Yune, T.Y., Lee, J.Y., Jung, G.Y., Kim, S.J., Jiang, M.H., Kim, Y.C., Oh, Y.J., Markelonis, G.J. & Oh, T.H. (2007) Minocycline alleviates death of oligodendrocytes by inhibiting pro-nerve growth factor production in microglia after spinal cord injury. *J. Neurosci.*, **27**, 7751–7761.

Zhu, X., Raina, A.K., Lee, H.G., Chao, M., Nunomura, A., Tabaton, M., Petersen, R.B., Perry, G. & Smith, M.A. (2003) Oxidative stress and neuronal adaptation in Alzheimer disease: the role of SAPK pathways. *Antioxid. Redox Signal.*, **5**, 571–576.